Non-stationary response of photorefractive crystal under an external sinusoidal electric field

O. Salas-Torres[a], A. Zúñiga-Segundo[a], and L.F. Magaña-Solís[b]
[a]*Departamento de Física, Escuela Superior de Física y Matemáticas, Edificio 9, Unidad Profesional Adolfo López Mateos, 07738, México, D.F., México.*
[b]*Instituto de Física, Universidad Nacional Autónoma de México, Apartado Postal 20-364, México, D.F., 01000 México.*

Recibido el 25 de abril de 2011; aceptado el 2 de marzo de 2012

We calculated the non-stationary holographic current arising in a photorefractive crystal illuminated by a vibrating sinusoidal pattern along with an external sinusoidal electric field applied to the sample. We first solved numerically the set of nonlinear material rate differential equations to find the full overall space charged field and the mobile carrier density for a photorefractive BSO crystal. With these results we calculated the photocurrent, which is found to be in good agreement with corresponding values obtained from holographic experiments performed with similar samples.

Keywords: Photorefractive gratings; photo-EMF; non-linear optics.

Calculamos la corriente que fluye en un cristal fotorefractivo cuando es iluminado por un patrón de interferencia móvil junto con un campo eléctrico externo sinusoidal. Resolvemos primeramente las ecuaciones diferenciales del cristal fotorefractivo BSO con el fin de encontrar el campo de carga espacial y la densidad de portadores móviles. Con estos resultados calculamos la corriente que fluye en el medio, encontramos una buena concordancia entre los valores obtenidos y los reportados en experimentos con muestras similares.

Descriptores: Rejillas fotorrefractivas; foto-FEM; óptica no lineal.

PACS: 42.70.Nq; 42.40.Eq; 42.40.Pa; 78.20.Jq

1. Introduction

The non-steady-state photo-electromotive force (photo-EMF) technique based on the detection of the alternating electric current arising in the sample illuminated by an oscillating interference pattern [1,2] is the most versatile and advanced method, used to determine the parameters of photo-induced charge carriers in semiconductors [1], non-crystalline materials [3], organic photo-conductors [4] and hybrid materials [5]. This method can be used to evaluate, for example, the mean photoconductivity σ of a crystal, the carrier diffusion length L_D, the mean carrier lifetime τ, the mobility μ, and the concentration of impurity centers N_A where the charge distribution is formed. On the other hand, the nonlinear effect of rectification of space charge waves (SCW) has been discovered in photo refractive crystals [6]. The SCW can be excited in semi-insulating crystals by optical means, particularly, during holographic recording of interference gratings in photorefractive crystals. Qualitatively, we can say the nonlinearity originates from the fact that the space charge field affects the formation of space charge grating. This effect led to changes in the dc current flowing through a crystal when SCW, are excited.

The most important feature of the above techniques is the interactions between the photo-induced space charge field grating and the grating of mobile photo-carriers which results in a periodic current flowing through the sample. The amplitude of the space-charge grating can be enhanced using the non-stationary mechanism of recording: the first approach uses application of a dc electric field to the crystal illuminated with a running interference pattern, (as in SCW excitation), the second one employs application of an ac electric field along with a stationary interference pattern. Thus, the study of the non-stationary holographic currents in an external alternating electric field [7], is useful not only for better understanding of the space charge field formation and characterization of the materials, but also for practical applications.

In this paper we calculate the photo-EMF in presence of an external sinusoidal electric field, we first calculate numerically the time evolution of the overall space charged field and the mobile carrier density for a photorefractive BSO crystal. Then we use the explicit expression for density current in terms of the above time-dependent solutions. In Sec. 2 we describe the basic equations for the non-stationary recording and photorefractive material rate equations. The experimental setup is described in Sec. 3 as was reported in Ref. 7. In Sec. 4 we present the numerical results of the non-stationary photocurrent simulations in n-type photorefractive BSO, and in section V we propose a modification of the photo-EMF technique to enhanced the photocurrent signal.

2. Theoretical background

We consider a photorefractive crystal placed into an external alternating electric field and illuminated by an oscillating interference pattern formed by two coherent laser beams, one of them is phase-modulated with a modulation frequency ω and amplitude Δ, as it seen in Fig. 1. The oscillating interference pattern is given by,

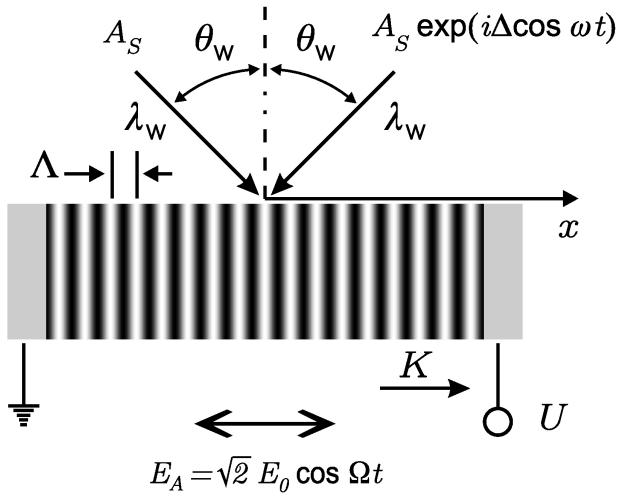

FIGURE 1. Schematic of the setup used. A BSO crystal is illuminated by a oscillating interference pattern along with an external sinusoidal electric field. The amplitude of the space-charge field is shown in gray scale.

$$I(x,t) = I_0[1 + m\cos(Kx + \Delta\cos\omega t)] \,, \qquad (1)$$

with I_0 the average light intensity, m the contrast of the interference pattern, x the transversal coordinate on the crystal, and $K = 2\pi/\Lambda$, where Λ is the interference pattern spacing. The alternating electric field is applied in the $\vec{K}$ direction by means of electrodes at the ends of the sample. For a symmetrical recording scheme we obtain,

$$\Lambda = \frac{\lambda_W}{2\sin\theta_W} \,, \qquad (2)$$

where λ_W is the recording light wavelength and θ_W is the angle of incidence of the recording beams. As it is well known, in photorefractive crystals a light pattern may be transposed into a refractive index pattern. Inhomogeneous illumination excites charge carriers into conduction or valence bands. The charge carriers migrate and holographic currents arise, and finally the carriers are trapped. Given that the excitation rate is smaller in the darker regions, the charge accumulates in the darker parts of the crystals. Due to this charge distribution a space charge field builds up and modulates the refractive index via the electro-optic effect. In this paper we consider the widely used model of semiconductor with one type of charge carriers (electrons) and one photoactive impurity level [8,9]. The differential equations in this model are the following.

$$\frac{\partial N_D^+}{\partial t} = (sI + \beta)(N_D - N_D^+) - \gamma n_e N_D^+ \,, \qquad (3)$$

$$\frac{\partial n_e}{\partial t} = \frac{\partial N_D^+}{\partial t} + \frac{\mu}{e}\frac{\partial}{\partial x}\left(D\frac{\partial n_e}{\partial x} + e n_e E\right) \,, \qquad (4)$$

$$\frac{\partial(\epsilon_o \epsilon E)}{\partial x} = e(N_D^+ - N_A - n_e) \,, \qquad (5)$$

where N_A, N_D, N_D^+ and n_e are the densities of compensating acceptors centers, donors, ionized donors and free electrons respectively; s is the light-excitation cross section, γ is the two-body recombination coefficient; β is the thermal-excitation rate; ϵ is the static dielectric constant, μ is the electron mobility; $D = k_B T$ with, k_B the Boltzmann's constant; T is the absolute temperature; e is the elementary charge and $E = E_A + E_{SC}$, with E_A is the external sinusoidal electric field $E_A = \sqrt{2}E_0\cos\Omega t$ with amplitude E_0 and frequency Ω; E_{SC} is the space-charge field. The experimental parameters [7] used in the BSO simulations are shown in Table I.

TABLE I. Experimental parameters for BSO crystal, from Ref. 7.

	BSO	
ϵ	Dielectric constant	56
n_0	Average refractive index	2.34
r_{eff}	Electro optic coefficient (mV^{-1})	4.7×10^{-12}
Λ	Fringe spacing (μm)	125.66
$\mu\tau$	Mobility lifetime product (m^2V^{-1})	1.2×10^{-10}
γ	Recombination constant (m^3s^{-1})	1.6×10^{-17}
β	Thermal-excitation rate	0
s	Photo ionization cross section (m^2J^{-1})	1.0×10^{-5}
N_D	Donor density (m^{-3})	10^{25}
N_A	Acceptor density (m^{-3})	10^{22}
Δ	Beam modulating amplitude	0.16

It is possible to show that the current density flowing through the electrodes at the end of the sample, along the direction of $\vec{K}$, can be written as

$$j(t) = \frac{1}{\Lambda}\int_0^{\Lambda} e\mu n_e(x,t)E(x,t)dx \,, \qquad (6)$$

where we have considered that for the sinusoidal interference pattern (stationary, running, or oscillating), we have periodic boundary conditions, so that the averaging can be performed only over one spatial grating period Λ [12].

3. Experimental setup

The typical experimental setup used to make measurements of the non-stationary holographic currents under applied alternating electric field is shown in Fig. 1, as reported in Ref. 7. Two laser beams with an average power I_0 =5.0 mW/cm, and a wavelength λ_W =442 nm were used for recording interference pattern with contrast m =0.65. A modulator produced phase modulation of the laser beam with frequency $\omega/2\pi$ =2000 Hz and amplitude Δ =0.16. The angle of incidence θ_W is given by the Bragg relation (2), we used a fringe spacing of Λ =125.6 microns ($K = 5\times10^4\text{m}^{-1}$) and an applied ac field with frequency $\Omega/2\pi$=6.0 kHz. The vector $\vec{K}$ is in the direction of the collecting electrodes *i.e.*, parallel to the applied field E_A as it seen in Fig. 1. Two silver paste electrodes 3×4 mm^2 were painted on the lateral surfaces where an amplified voltage U

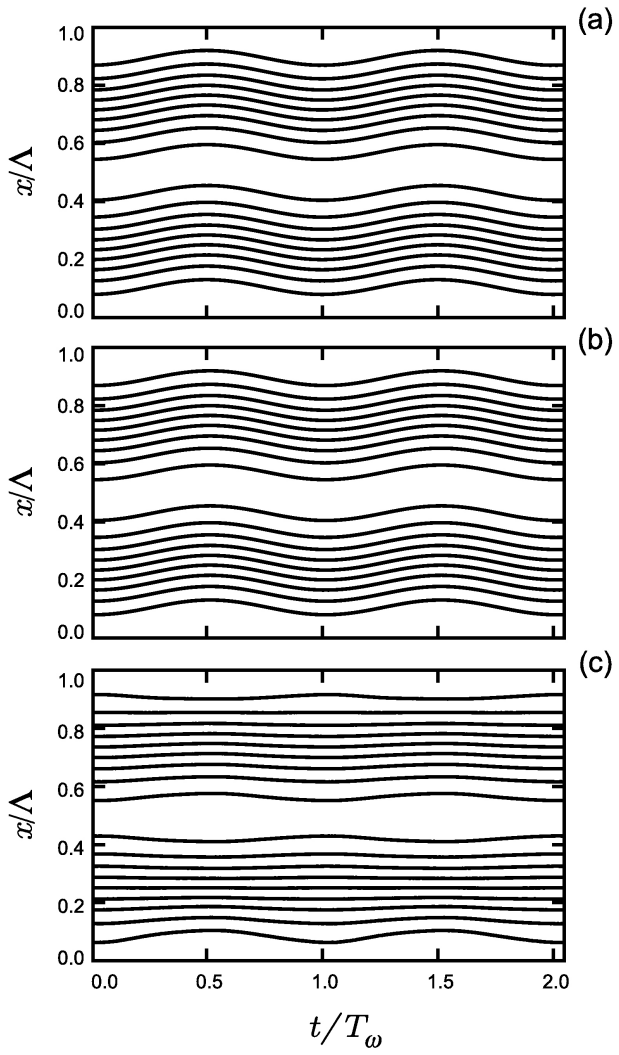

FIGURE 2. Contour plots of the time evolution of: (a) a oscillating interference pattern $I(x,t)$, (b) a carrier grating $n_e(x,t)$ when the applied field amplitude is $E_0 = 0$, (c) a carrier grating $n_e(x,t)$ when the applied field amplitude is $E_0 = 10$ kV/cm.

was applied to the sample. A surface of 1×10 mm^2 was illuminated by the oscillating fringe pattern.

4. Numerical results

We start by analyzing in detail the time evolution of $I(x,t)$, $n_e(x,t)$, $E_{SC}(x,t)$ and $N_D^+(x,t)$ during dynamic photorefractive recording by solving numerically the nonlinear material rate differential Eqs. (3-5) (details are given in Refs. 10 and 11). The incident light excites photo-carriers (electrons in our case) in accordance with the equation (1), resulting in several charge gratings. Some of them are gratings of free carriers and others are gratings of ionized traps, and can be united under the so-called "space-charge gratings" [12]. In the next figures we will consider the time within the interval $(0, 2T_\omega)$ after a stabilization time of 4.0 seconds (we assume for simplicity that the "space-charge gratings"have reached stable oscillations by the end of this time interval). Also, for the sake of simplicity, the transverse coordinate x and time t were scaled to the grating period Λ and time period $T_\omega = 2\pi/\omega$ respectively.

The recording interference pattern contains a moving part proportional to $\exp(\pm i(Kx - \omega t))$, as shown in Fig. 2(a), where we display the contour plot of the scaled interference pattern $I(x,t)/I_0$. Figure 2(b) shows the free carrier oscillating grating ($n_e(x,t)$) moving in the same direction as the interference pattern, when the applied field amplitude E_0=0.

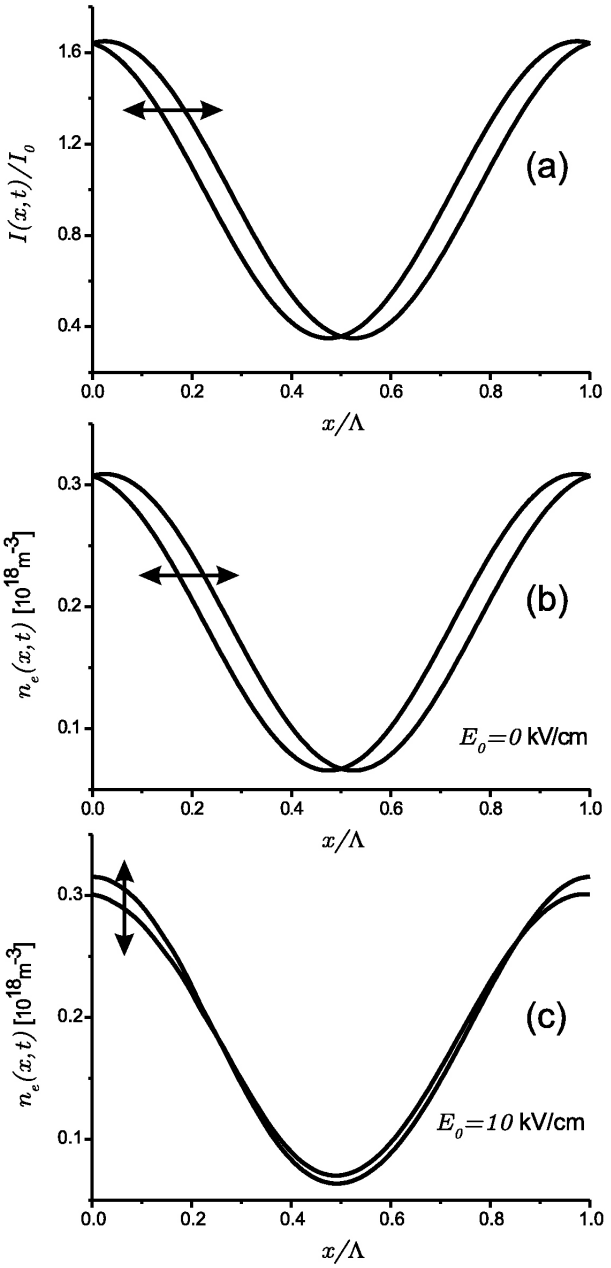

FIGURE 3. Transverse time evolution of: (a) a oscillating interference pattern $I(x,t)$, (b) a carrier grating $n_e(x,t)$ when the applied field amplitude is $E_0 = 0$, (c) a carrier grating $n_e(x,t)$ when the applied field amplitude is $E_0 = 10$ kV/cm. In all cases the respective function "bounces" along the double arrow direction between its boundary values

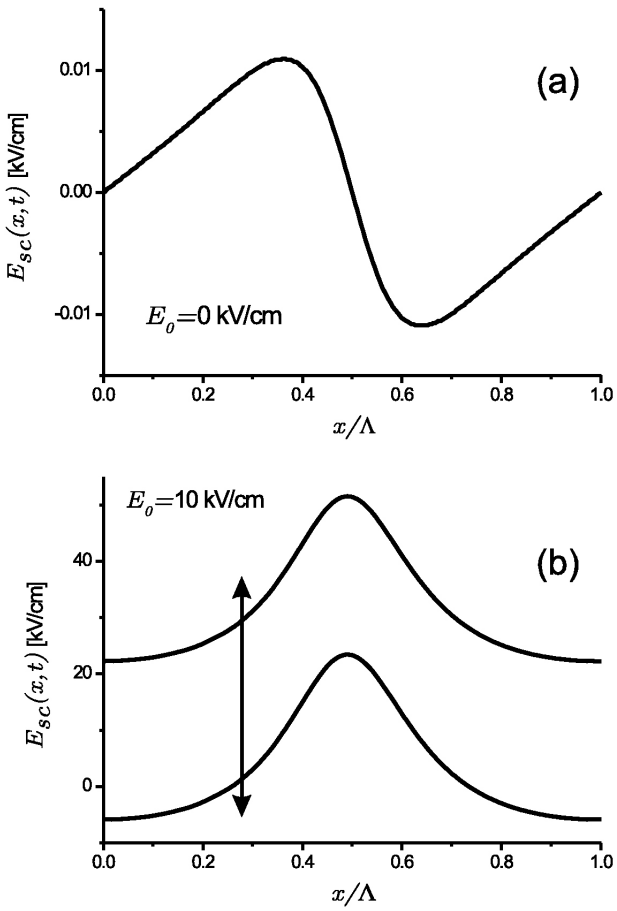

FIGURE 4. Transverse time evolution of space-charge field grating $E_{\rm SC}(x,t)$ when the applied field amplitude is: (a) $E_0 = 0$, (b) $E_0 = 10$ kV/cm. The $E_{\rm SC}(x,t)$ "bounces" along the double arrow direction, between its two boundary values.

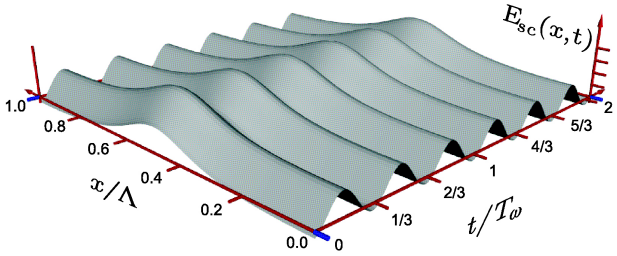

FIGURE 5. Three-dimensional plot which shows the time evolution of space-charge field grating $E_{\rm SC}(x,t)$ when the applied field amplitude $E_0 = 10$ kV/cm.

If the applied field amplitude increases we observe that the carrier oscillating grating moving is quite complicated; in some regions it is moving in the opposite direction to the interference pattern, but in others regions it is practically static as shown in Fig. 2(c) with nearly straight lines, when the applied field amplitude is E_0 =10 kV/cm.

Alternatively we can use Fig. 3(a) to show how the scaled oscillating pattern $I(x,t)/I_0$ oscillates horizontally between its left and right boundary values, (like a squash ball bounces between two walls), with a well-defined frequency and amplitude. The double arrow indicates the path followed by the oscillating pattern. Similar movement has been carried out for carrier grating $n_e(x,t)$ when the applied field amplitude is $E_0 = 0$, as is shown in Fig. 3(b); in fact Figs. 3(a) and 3(b) are the same under an adequate scaled factor, now the double arrow indicates the path followed by the carrier grating. We can see that with increasing applied field amplitude (E_0=10 kV/cm) the carrier grating oscillates vertically and is constrained to move between its down and top boundary values, with a well-defined frequency but different amplitudes and opposite directions, as shown in the central region of Fig. 3(c); this explains the asymmetric shape of the figure.

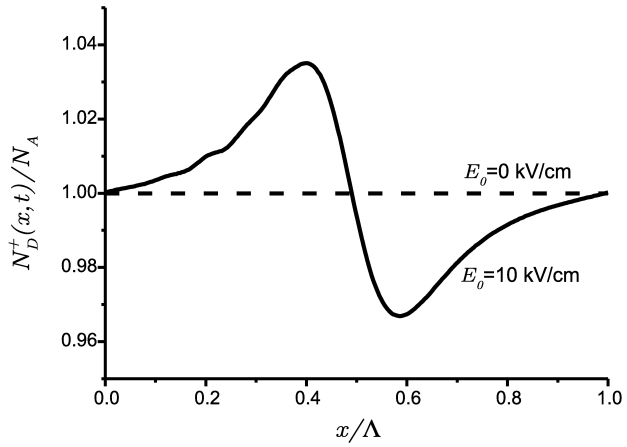

FIGURE 6. Transverse time evolution of the ionized donors grating $N_D^+(x,t)$, when the applied field amplitude is: (a) $E_0 = 0$, shown by the dotted line, (b) $E_0 = 10$ kV/cm.

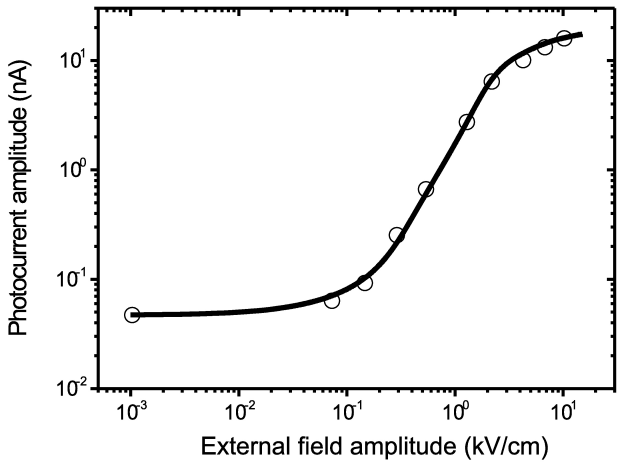

FIGURE 7. Photocurrent amplitude versus applied field amplitude, when the modulating frequency is $\omega/2\pi$ =2000 Hz. The circles represent experimental data. The solid line is our numerical estimation.

The time evolution of the space-charge field grating $E_{\rm SC}(x,t)$ is plotted in Fig. 4. When the applied field amplitude is $E_0 = 0$, the grating is static and its amplitude is very small (of the order of 10^{-2} kV/cm) as seen in Fig. 4(a). However if we increase the applied field amplitude, $E_{\rm SC}(x,t)$

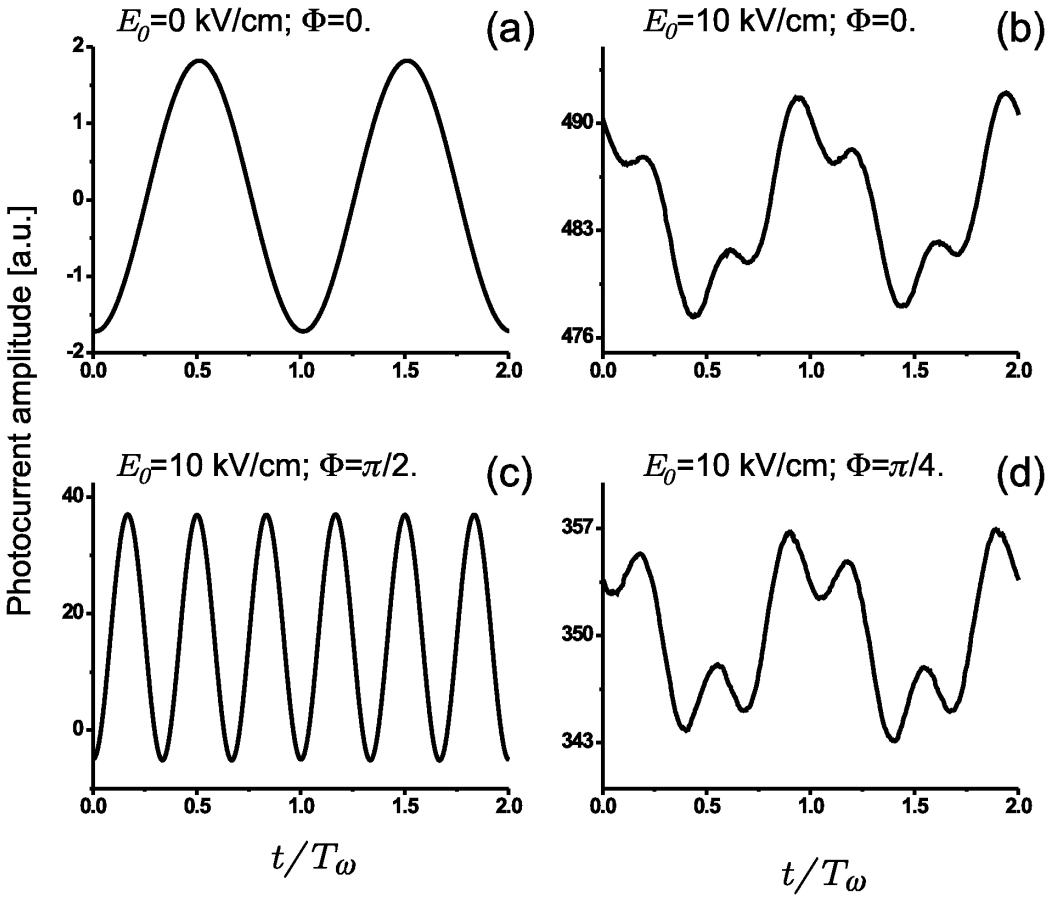

FIGURE 8. Time evolution of photocurrent amplitude and photo-EMF, for different values of the applied field $E_A=\sqrt{2}E_0\cos(\Omega t+\Phi)$, when: (a) $E_0 = 0$ kV/cm, $\Phi = 0$, (b) $E_0 = 10$ kV/cm, $\Phi = 0$, (c) $E_0 = 10$ kV/cm, $\Phi = \pi/2$, (d) $E_0 = 10$ kV/cm, $\Phi = \pi/4$.

grows as E_0^2 until saturation is reached, and oscillates vertically while keeping its shape, as is shown in Fig. 4(b), where the double arrow indicates the path followed by the charge field grating when the applied field amplitude E_0=10 kV/cm. More details of the time evolution of this grating are shown in Fig. 5, where with the help of a three-dimensional surface plot we can clearly see that $E_{\rm SC}(x,t)$ is forced to oscillate at the applied field frequency Ω.

The above simulations suggest that the space charge grating should be key to the non-stationary photorefractive recording, and its "gate" will be the applied field amplitude. When $E_0 = 0$ the space charge field $E_{\rm SC}(x,t)$ is small and the carrier grating $n_e(x,t)$ follows the pattern grating. In other cases, when $E_0 \neq 0$, the space charge field is high and the carrier grating follows the space charge grating, as seen in Fig. 3(c).

In order to have a complete picture of the "space-charge gratings" we also report the ionized donor's grating $N_D^+(x,t)$, which is stationary for all values of applied field amplitude, as shown in Fig. 6. When E_0=0, $N_D^+(x,t)$=N_A (see the dotted line) nevertheless if $E_0 = 10$ kV/cm $N_D^+(x,t) \approx N_A$, *i.e.*, N_D^+ is slightly different from N_A.

Finally in Fig. 7 we show our results for the photo-EMF, as function of the external field amplitude E_0. The open circles (○) represent the experimental data from Ref. 7. The solid line is our theoretical calculation in accordance with the effective value (RMS) of (6) multiplied by the lateral area surface. One can see a quite reasonable agreement between theoretical and experimental data. The photo-EMF was obtained from the solutions $n_e(x,t)$, $E_{SC}(x,t)$ of the nonlinear material rate differential Eqs. (3-5) for time 4.0 seconds.

5. Discusion

It is known that the utilization of ac fields for the enhancement of photocurrent signals provides several important advantages over the application of a dc field. One of those attractive features is the giant signal enhancement, which it has been derived assuming an ad hoc applied field equation $E_A = \sqrt{2}E_0\cos\Omega t$. A question is raised by this result: Would an additional phase in the applied field destroy this enhancement? In this section we show the effect of this phase in the photocurrent. Figure 8 shows the strong dependence of the photocurrent when an additional phase is introducing in the alternating applied field as $E_A = \sqrt{2}E_0\cos(\Omega t + \Phi)$. In case of the phase $\Phi = 0$, we have the results reported above, as seen in Figs. 8(a) and 8(b). In Fig. 8(a) when the applied

field amplitude is $E_0 = 0$ the photocurrent has the same frequency of the oscillating pattern grating. This result may be viewed as a consequence of the fact that $n_e(x,t)$ follows the pattern grating $I(x,t)$ and $E_{SC}(x,t)$ is small and stationary and it does not give any contribution to the photo-EMF. When $E_0 \neq 0$ the space-charge field is high and it does give a dominant contribution to the photo-EMF as shown in Fig. 8(b). If $E_0 \neq 0$ and the phase was $\Phi = \pi/2$, the space-charge field $E_{SC}(x,t)$ gives a dominant contribution to the photocurrent, but in this case the photocurrent drops dramatically (and the photo-EMF grows) as it seen in Fig. 8(c). Finally when the phase is $\Phi = \pi/4$, the photocurrent grows again and both $n_e(x,t)$ and $E_{SC}(x,t)$ have contributions to the photocurrent as shown in Fig. 8(d).

Our numerical experiments show a sensitive behaviour of photo-EMF which is attributed to additional phase in the alternating applied field. We believe that this phase may be included externally or by means of feedback loop to improve this technique

6. Acknowledgments

A.Z.S. would like to thank S. Barraza-López (UARK), A. Khomenko and N. Korneev for their fruitful discussions, as well as H. Moya-Cessa for his hospitality at INAOE where these ideas were developed. We thank SIP-IPN grant 20120303.

1. M.P. Petrov, I.A. Sokolov, S.I. Stepanov, and G.S. Trofimov, *J. Appl. Phys.* **68** (1990) 216.
2. I.A. Sokolov and S.I. Stepanov, *J. Opt. Soc. Am. B* **10** (1993) 1483.
3. M. Bryushinin, V. Golubev, Y. Kumzerov, D. Kurdyukov, and I. Sokolov, *Applied Physics B: Lasers and Optics* **95** (2009) 489.
4. M. C. Gather, S. Mansurova, and K. Meerholz, *Phys. Rev. B* **75** (2007) 165203.
5. S. Mansurova, K. Meerholz, E. Sliwinska, U. Hartwig, and K. Buse, *Phys. Rev. B* **79** (2009) 174208.
6. M.P. Petrov, V.V. Bryksin, H. Vogt, F. Rahe, and E. Krätzig, *Phys. Rev. B* **66** (2002) 085107.
7. M. Bryushinin, V. Kulikov, and I. Sokolov, *Phys. Rev. B* **65** (2002) 245204.
8. N.V. Kukhtarev, V.B. Markov, S.G. Odulov, M.S. Soskin, and V.L. Vinetskii, *Ferroelectrics* **23** (1979) 949.
9. N.V. Kukhtarev, T. Kukhtareva, and P.P. Banerjee, *Proceedings of the IEEE* **87** (1999) 1857.
10. L.F. Magaña, I. Casar and J.G. Murillo, *Opt. Mater.* **30** (2008) 979.
11. J.G. Murillo, L.F. Magaña, M. Carrascosa, and F. Agulló-López, *J. Appl. Phys.* **78** (1995) 5686.
12. S.I. Stepanov, "*Photo-electromotive-force effect in semiconductors*", in Semiconductor Devices, H. S. Nalwa, ed., Vol. 2 of Handbook of Advanced Electronic and Photonic Materials and Devices, Chap. 6, (Academic, San Diego, Calif., 2001) pp. 205-272.